

Transport properties of double-walled carbon nanotube quantum dots

Shidong Wang and Milena Grifoni

Theoretische Physik, Universität Regensburg, 93040 Regensburg, Germany.

(Dated: November 30, 2018)

The transport properties of quantum dot (QD) systems based on double-walled carbon nanotube (DWCNT) are investigated. The interplay between microscopic structure and strong Coulomb interaction is treated within a bosonization framework. The linear and nonlinear G - V - V_g characteristics of the QD system is calculated by starting from the Liouville equation for the reduced density matrix. Depending on the intershell couplings, an 8-electron periodicity of the Coulomb blockade peak spacing in the case of commensurate DWCNT QDs and a 4-electron periodicity in the incommensurate case are predicted. The contribution of excited states of DWCNTs to the nonlinear transport is investigated as well.

PACS numbers: 73.63.Fg, 73.23.Hk, 71.10.Pm

I. INTRODUCTION

After being discovered in 1991¹, carbon nanotubes (CNTs) have been widely used in nano-devices because of their unique properties^{2,3,4}. CNTs may be either single-walled (SWCNT) or multi-walled (MWCNT) depending on the number of graphene sheets wrapped into concentric cylinders. Due to the quasi-one-dimensional characters of their electronic structures, long SWCNTs exhibit Luttinger-liquid behavior^{5,6,7,8,9}. SWCNT quantum dot (QD) systems have also been fabricated, which consist of finite length SWCNTs weakly connected to the source and drain leads and capacitively coupled to a gate electrode^{10,11,12,13}. At low bias, the SWCNT QD systems show Coulomb blockade behavior because of the strong Coulomb interactions in the QDs and the poor transparencies of the contacts between the QD and the leads¹⁴. Because of the short lengths of SWCNTs, the addition energy needed to add an extra electron to the QD depends on both the Coulomb interaction and on the energy level spacing. Unlike the traditional two-dimensional semiconductor QD systems with irregular Coulomb blockade patterns, which have to be understood statistically¹⁵, QDs based on SWCNTs show regular Coulomb blockade patterns, which originate from the regular electronic structure of the SWCNTs. Because of the spin degeneracy of two bands crossing at the Fermi points in metallic SWCNTs, the stability diagrams of SWCNT QD systems exhibit a 4-electron periodicity of the Coulomb diamond sizes^{10,11,12,13,16}. The stability diagrams of the SWCNT QD systems have been explained by using the mean-field theory developed in Ref. 17 which includes a nonzero exchange energy^{10,11,12,13}. Recently, the energy spectrum of SWCNT QD has been calculated in Refs. 18 and 19 beyond mean field. For QD systems with moderate-to-large radius SWCNTs, the exchange energy can be ignored²⁰, and the stability diagrams can also be quantitatively explained within a bosonization approach^{18,19}. By suitable choice of parameters these theories can reproduce the *same* low bias spectra of SWCNT QDs, and only the excitations measured at high bias are predicted differently by a mean-field approach or by a bosonization method because of the different treatment of the Coulomb interaction¹⁹. Although the excitations of SWCNT QDs have already been measured¹², the quality and the range of the measured excitations cannot be used to determine the validity of these two methods and further experiments are needed.

So far, the properties of MWCNT QD systems have not been fully explored²¹. The experiment in Ref. 21 showed that the stability diagrams of MWCNT QD systems have a 4-electron periodicity of the Coulomb diamond sizes. The simplest MWCNT QD is the one formed by a double-walled carbon nanotube (DWCNT), which consists of two concentric shells. Depending on the ratio between the unit cell lengths of the two shells, a DWCNT may be either commensurate (c-DWCNT), if the ratio is a commensurate number, or incommensurate (i-DWCNT), if the ratio is an incommensurate number. It has been shown that the effective intershell coupling depends on the type of DWCNTs. At low energies, that is, near the Fermi energy, the effective intershell coupling is negligible in i-DWCNTs but large in c-DWCNTs while it cannot be ignored in both type of DWCNTs at high energies^{22,23,24,25}. Both types of DWCNTs with long lengths can be described by Luttinger liquid theory when Coulomb interactions are included^{25,26}. Because of their intermediate-to-large radii, we expect that the exchange energy may be ignored in DWCNTs. Therefore, the bosonization approach, which includes forward scattering processes exactly, can be used to describe the properties of DWCNT QD systems as well.

In this paper, we consider a QD system formed by a finite length DWCNT with two metallic shells, where we include all forward scattering processes. The bosonization approach enables exact diagonalization of the interacting DWCNT Hamiltonian. Finally, the linear and nonlinear transport properties of the system are investigated by solving the Liouville equation for the reduced density matrix to lowest order in the coupling to the leads.

The paper is organized as follows. In Sec. II, the Hamiltonian of a DWCNT QD system is derived. The energy

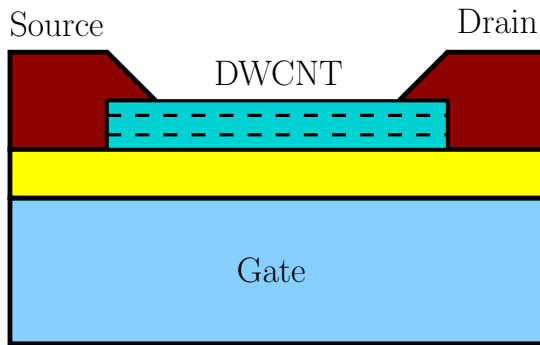


FIG. 1: (Color online) Schematic experimental setup of a double-walled carbon nanotube (DWCNT) quantum dot (QD) system. A finite length DWCNT is deposited on a substrate and weakly connected to the source and drain leads through its outer shell. A gate electrode is capacitively coupled to the DWCNT QD and controls the electrochemical potential in the QD. The dashed lines denote the inner shell in the DWCNT.

spectrum of a finite length DWCNT with strong Coulomb interactions and open boundary conditions is then obtained. Transport properties of DWCNT QDs are calculated in Sec. III. The results for the linear and nonlinear conductances of both *c*-DWCNT and *i*-DWCNT QDs are presented in Sec. IV. Finally, the conclusion is drawn in Sec. V.

II. MODEL AND METHOD

As schematically shown in Fig. 1, the QD system consists of a DWCNT with two metallic shells deposited on a substrate. The source and drain leads are connected to the outer shell of the DWCNT. The segment of the DWCNT (of about several hundred nanometers long) between two leads forms a QD. A gate electrode is capacitively coupled to the QD and controls the electrochemical potential in it. As we are only interested in the Coulomb blockade regime, we assume that the QD is weakly contacted to two leads, that is, the transparencies of the contacts are very poor and the conductance of the QD system is much smaller than the conductance quantum $2e^2/h$. The Hamiltonian of the whole system can be separated into several parts,

$$H = H_{\text{leads}} + H_{QD} + H_T + H_g, \quad (1)$$

where H_{QD} is the Hamiltonian of the QD system and its explicit form will be derived in the following subsection. The source (*s*) and drain (*d*) leads are described by Fermi gases of non-interacting quasi-particles and the Hamiltonian of the leads is

$$H_{\text{leads}} = \sum_{l=s,d} \sum_{\mathbf{k}\sigma} (\varepsilon_{l\mathbf{k}} - eV_l) c_{l\mathbf{k}\sigma}^\dagger c_{l\mathbf{k}\sigma}, \quad (2)$$

where e is the elementary charge and V_l is the voltage in the lead l . The operators $c_{l\mathbf{k}\sigma}^\dagger$ and $c_{l\mathbf{k}\sigma}$ are the creation and annihilation operators of a quasi-particle with wave vector \mathbf{k} and spin $\sigma = \pm$ in the lead l . The Hamiltonian of the gate is

$$H_g = -e\mu_g \mathcal{N},$$

where μ_g is the chemical potential in the gate and the operator \mathcal{N} accounts for the total number in the QD system. H_T is the tunneling Hamiltonian describing the tunneling between the QD and the two leads and it has the form

$$H_T = \sum_{l=s,d} \sum_{\beta\sigma} \int d\mathbf{r} T_{l\beta}(\mathbf{r}) \Psi_{\beta\sigma}^\dagger(\mathbf{r}) \Phi_{l\sigma}(\mathbf{r}) + \text{H.c.}, \quad (3)$$

where $\Phi_{l\sigma}(\mathbf{r}) = \sum_{\mathbf{k}} \phi_{\mathbf{k}}(\mathbf{r}) c_{\mathbf{k}l\sigma}$ is the electron annihilation operator in the lead l and $\Psi_{\beta\sigma}^\dagger(\mathbf{r})$ is the electron operator in the shell β whose explicit form will be given in Sec. II A.

A. Low energy non-interacting Hamiltonian of DWCNT

In general, the energy spectrum of a SWCNT or of a DWCNT without electron-electron interactions can be obtained by using a tight-binding model for the p_z orbitals in carbon atoms². In particular, we shall view in the following a

DWCNT as two tunneling coupled SWCNT shells. We denote with the index $\beta = \pm$ the outer/inner SWCNT shell. A metallic SWCNT shell β within periodic boundary conditions has two independent Fermi points ($\pm K_{0,\beta}$). Their positions depend on the chirality of the shell and in general are different for different SWCNT shells. At the Fermi points, the lowest conduction and the highest valence bands touch each other as shown in Fig. 2(a). As the next conduction and valence bands are separated by a large gap (about 1 eV)², we will only consider the lowest conduction band and the highest valence band in our calculations. The energy dispersion near the Fermi points is linear², see Fig. 2(a), and is given by

$$\varepsilon_{R/L}(\kappa) = \pm \hbar v_F \kappa, \quad (4)$$

where the wave vector κ is measured with respect to the Fermi points and the Fermi velocity in SWCNTs is $v_F \approx 8 \times 10^5$ m/s. Hence, at each Fermi point, there are two branches corresponding to the right (+) and left (-) moving electrons. The Bloch waves for the electrons in these branches in a shell $\beta = \pm$ are

$$\varphi_{\beta r F \kappa}(\mathbf{r}) = e^{i\kappa u} \varphi_{\beta r F}(\mathbf{r}), \quad (5)$$

where $\mathbf{r} = (u, v)$ and u and v are along the nanotube axis and the circumference directions, respectively (cf. Fig. 3). The index $r = R/L = \pm$ denotes the right and left-moving electrons. The periodic function is

$$\varphi_{\beta r F}(\mathbf{r}) = \frac{1}{\sqrt{N_\beta}} \sum_{\mathbf{R}p} e^{i\mathbf{F} \cdot \mathbf{R}} f_{\beta p r F} \chi(\mathbf{r} - \mathbf{R} - \boldsymbol{\tau}_p), \quad (6)$$

where the index \mathbf{R} denotes the lattice vector of the graphene sheet, N_β is the number of carbon atoms in the shell β , p is the index for the two graphene sublattices and $\boldsymbol{\tau}_p$ is the vector giving the positions of the two different atoms in a unit cell. The index F is for the Fermi points in the shell and \mathbf{F} denotes the Fermi points in a graphene sheet. They are related as $F \equiv \mathbf{F} \cdot \mathbf{u}$ with \mathbf{u} the unit vector along the nanotube axis. The coefficients f 's depend on the chirality of the shell (m, n) as²

$$f_{\beta A r F} = \frac{1}{\sqrt{2}\mathcal{L}} \left(-\frac{\sqrt{3}}{2} \text{sgn}(Fr)(n+m) + \frac{i}{2} \text{sgn}(r)(m-n) \right), \quad (7)$$

$$f_{\beta B r F} = \frac{1}{\sqrt{2}}. \quad (8)$$

where $\mathcal{L} = \sqrt{n^2 + mn + m^2}$ and the function $\chi(\mathbf{r} - \mathbf{R})$ is the p_z orbital wave function. Because we consider a finite length shell, we have to use the open boundary condition (OBC) instead of the periodic boundary condition along the tube axis (cf. Fig. 4). The wave function in the shell β satisfying the OBC has the form¹⁹

$$\varphi_{\beta \tilde{R}/\tilde{L}\kappa}^{OBC}(\mathbf{r}) = \frac{1}{\sqrt{2}} \left(\varphi_{\beta R/L K_0 \kappa}(\mathbf{r}) - \varphi_{\beta L/R -K_0 -\kappa}(\mathbf{r}) \right), \quad (9)$$

and the wave vectors κ are quantized as

$$\kappa = \frac{\pi}{L} (m_\kappa + \Delta_\beta), \quad m_\kappa = 0, \pm 1, \pm 2, \dots, \quad (10)$$

where L is the length of the nanotube. The mismatch of the Fermi points is $0 \leq \Delta_\beta = K_{0,\beta} L / \pi - [K_{0,\beta} L / \pi] < 1$, where $[\dots]$ gives the integer part of its argument. The Hamiltonian of a finite length non-interacting shell β is thus

$$H_\beta^0 = \sum_{\tilde{r}\sigma\kappa} \text{sgn}(\tilde{r}) \hbar v_F \kappa c_{\beta \tilde{r}\kappa\sigma}^\dagger c_{\beta \tilde{r}\kappa\sigma}, \quad (11)$$

where $\tilde{r} = \tilde{R}/\tilde{L} = \pm$ is the index for the left and right moving electrons with the OBC. The operators $c_{\beta \tilde{r}\kappa\sigma}^\dagger$ and $c_{\beta \tilde{r}\kappa\sigma}$ are the creation and annihilation operators of an electron in the branch \tilde{r} with the wave vector κ and spin σ .

Let us now see how the spectrum gets modified when looking at DWCNT. At low energies, the intershell couplings are different for c-DWCNTs and i-DWCNTs. The intershell couplings in i-DWCNTs are negligible while they are quite strong in c-DWCNTs^{22,23,25,27,28,29}. Therefore, the non-interacting Hamiltonian of an i-DWCNT is the combination of the Hamiltonians of two shells,

$$\begin{aligned} H_{i\text{-DWCNT}}^0 &= \sum_{\beta \tilde{r}\sigma\kappa} \text{sgn}(\tilde{r}) \hbar v_F \kappa c_{\beta \tilde{r}\kappa\sigma}^\dagger c_{\beta \tilde{r}\kappa\sigma} \\ &= \sum_{\beta \tilde{r}\sigma m_\kappa} \text{sgn}(\tilde{r}) (m_\kappa \varepsilon_0 + \Delta_\beta \varepsilon_0) c_{\beta \tilde{r}\kappa\sigma}^\dagger c_{\beta \tilde{r}\kappa\sigma}, \end{aligned} \quad (12)$$

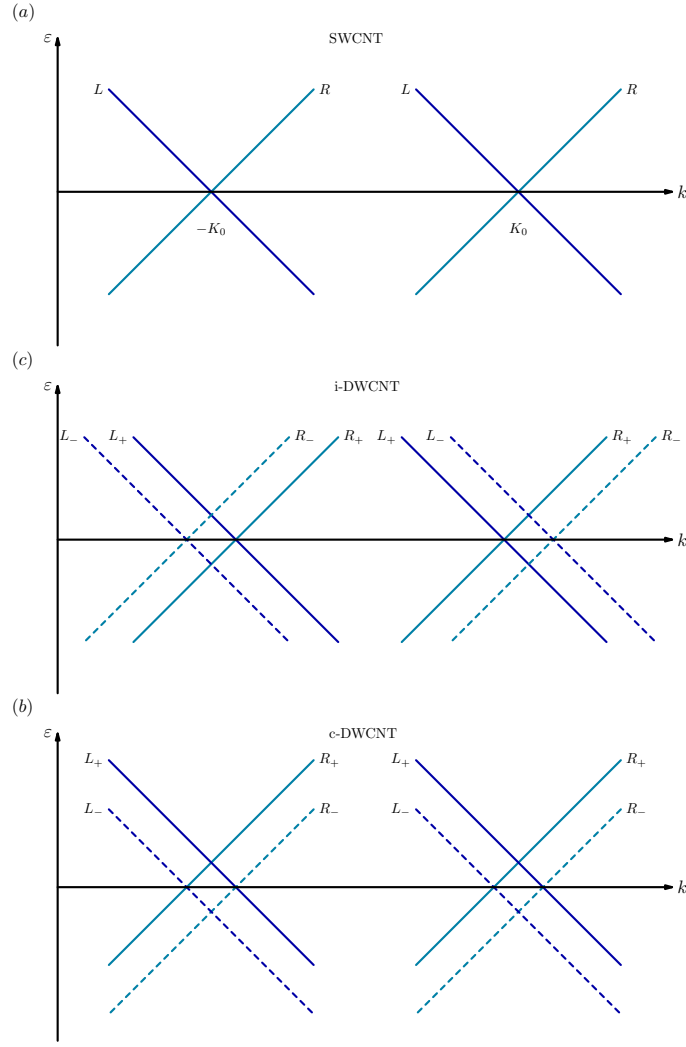


FIG. 2: (Color online) Energy spectra of metallic single-walled (SWCNT) and double-walled (DWCNT) carbon nanotubes with *periodic* boundary conditions (PBC). (a) Energy spectrum of a metallic SWCNT. There are two Fermi points and two branches L/R with left/right-moving electrons at each the Fermi point. (b) Energy spectrum of an incommensurate DWCNT (i-DWCNT). It consists of the energy spectra of the outer and inner graphene shells (\pm), which are not coupled to each other because of the vanishing intershell coupling, cf. Eq. (12). (c) Energy spectrum of a commensurate DWCNT (c-DWCNT). Because of the finite intershell coupling, it is composed of the bonding and anti-bonding bands (\pm), which are shift vertically along the ε -axis, cf. Eq. (15).

where $\varepsilon_0 = \hbar v_F \pi / L$ is the level spacing and we have used the quantization relation for κ , Eq. (10) (cf. Fig. 4(b)). On the other hand, the non-interacting Hamiltonian of a c-DWCNT contains also the contribution from the intershell coupling²⁵,

$$H_{\text{c-DWCNT}}^0 = \sum_{\beta} \sum_{\tilde{r}\sigma\kappa} \text{sgn}(\tilde{r}) \hbar v_F \kappa c_{\beta\tilde{r}\kappa\sigma}^{\dagger} c_{\beta\tilde{r}\kappa\sigma} + \sum_{\beta\beta'} \sum_{\tilde{r}\sigma\kappa} t c_{\beta\tilde{r}\kappa\sigma}^{\dagger} c_{\beta'\tilde{r}\kappa\sigma} + \text{H.c.}, \quad (13)$$

where t is the intershell coupling and we assume that it is a constant in the low energy regime. The Hamiltonian Eq. (13) can be diagonalized by using the bonding and anti-bonding basis,

$$\tilde{c}_{\nu\tilde{r}\kappa\sigma} = \frac{1}{\sqrt{2}}(c_{+\tilde{r}\kappa\sigma} + \text{sgn}(\nu)c_{-\tilde{r}\kappa\sigma}), \quad \tilde{c}_{\nu\tilde{r}\kappa\sigma}^{\dagger} = \frac{1}{\sqrt{2}}(c_{+\tilde{r}\kappa\sigma}^{\dagger} + \text{sgn}(\nu)c_{-\tilde{r}\kappa\sigma}^{\dagger}), \quad (14)$$

where $\nu = \pm$ is the index for bonding and anti-bonding states, respectively. The non-interacting Hamiltonian of a

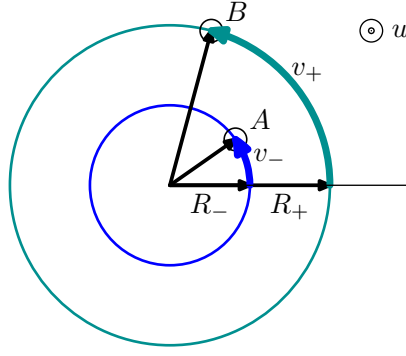


FIG. 3: (Color online) Cross section of a DWCNT. Atoms A and B in two shells of radii R_+ and R_- , respectively, are projected onto this cross section. Such atoms are described by the coordinates (u_+, v_+) and (u_-, v_-) , where u_{\pm} are along the tube axis and v_{\pm} measure the atom positions on the outer/inner circumference.

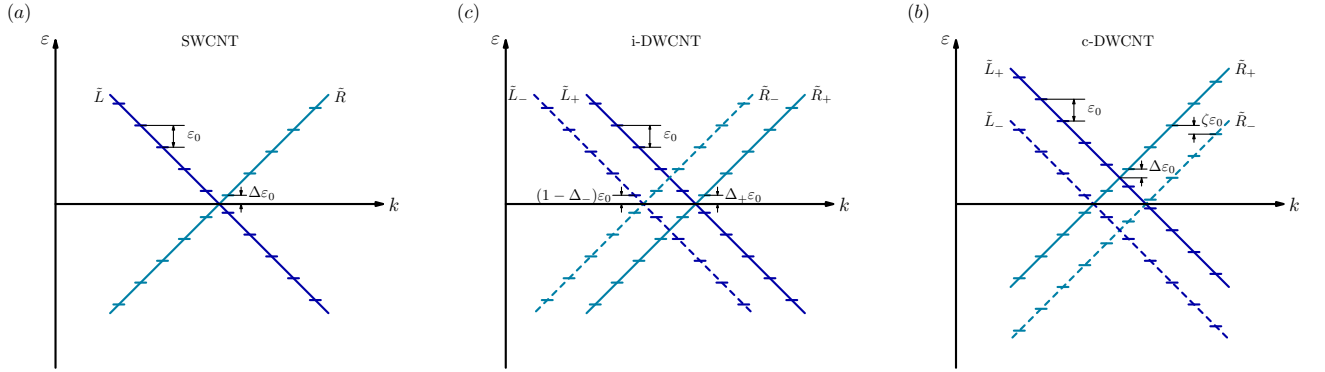


FIG. 4: (Color online) Energy spectra of metallic single-walled (SWCNT) and double-walled (DWCNT) carbon nanotubes with *open* boundary conditions (OBC). (a) Energy spectrum of a metallic SWCNT. There are two branches \tilde{L}/\tilde{R} with left/right-moving electrons. The parameter ε_0 is the level spacing and Δ describes the mismatch of the Fermi point, cf. Eq. (10). (b) Energy spectrum of a commensurate DWCNT (c-DWCNT) and (c) of an incommensurate DWCNT (i-DWCNT). The parameter Δ_{\pm} describes the mismatch of the Fermi point in the shell \pm and for a c-DWCNT is $\Delta_+ = \Delta_- = \Delta$. The parameter ζ describes the mismatch of the states in two bands, cf. Eq. (16).

c-DWCNT in the new basis becomes

$$\begin{aligned} H_{\text{c-DWCNT}}^0 &= \sum_{\nu\tilde{r}\sigma\kappa} (\text{sgn}(\tilde{r})\hbar v_F \kappa + \text{sgn}(\nu)t) \tilde{c}_{\tilde{r}\nu\kappa\sigma}^\dagger \tilde{c}_{\tilde{r}\nu\kappa\sigma} \\ &= \sum_{\nu\tilde{r}\sigma m_\kappa} (\text{sgn}(\tilde{r})(m_\kappa \varepsilon_0 + \Delta \varepsilon_0) + \text{sgn}(\nu)\zeta \varepsilon_0) \tilde{c}_{\tilde{r}\nu\kappa\sigma}^\dagger \tilde{c}_{\tilde{r}\nu\kappa\sigma}. \end{aligned} \quad (15)$$

where for c-DWCNT is $\Delta_\beta = \Delta$ and the parameter ζ is defined as

$$0 \leq \zeta = t/\varepsilon_0 - [t/\varepsilon_0] < 1, \quad (16)$$

which describes the mismatch of states in two bands (cf. Fig. 4(c)).

B. Coulomb interaction Hamiltonian of DWCNTs

In quasi-one dimensional electronic structures as CNTs, Coulomb interactions are not fully screened and can strongly influence the properties of CNTs^{5,6,7,8,9,25,26}. The total Coulomb interactions in an i-DWCNT can be expressed by the following Hamiltonian,

$$H_{\text{i-DWCNT}}^{\text{int}} = \frac{1}{2} \sum_{\beta'\sigma\sigma'} \iint d\mathbf{r}_1 d\mathbf{r}_2 \Psi_{\beta\sigma}^\dagger(\mathbf{r}_1) \Psi_{\beta'\sigma'}^\dagger(\mathbf{r}_2) U_{\beta\beta'}(\mathbf{r}_1 - \mathbf{r}_2) \Psi_{\beta'\sigma'}(\mathbf{r}_2) \Psi_{\beta\sigma}(\mathbf{r}_1), \quad (17)$$

where $\mathbf{r}_i = (u_i, v_i)$ and u and v are along the tube axis and the circumference direction, respectively (cf. Fig. 3). The intrashell interaction is given as

$$U_{\beta\beta}(\mathbf{r}_1 - \mathbf{r}_2) = \frac{e^2/\epsilon}{\sqrt{(u_1 - u_2)^2 + 4R_\beta^2 \sin^2((v_1 - v_2)/2R_\beta) + a_z^2}}, \quad (18)$$

and the intershell interaction is

$$U_{+-}(\mathbf{r}_1 - \mathbf{r}_2) = \frac{e^2/\epsilon}{\sqrt{(u_1 - u_2)^2 + 4R_+R_- \sin^2(v_1/2R_+ - v_2/2R_-) + \Delta R^2}}, \quad (19)$$

where ϵ is the dielectric constant, a_z is the ‘‘thickness’’ of a graphene sheet and the distance between two shells is $\Delta R = |R_+ - R_-|$. The electron operators for i-DWCNTs are defined as

$$\Psi_{\beta\sigma}(\mathbf{r}) \equiv \sum_{\tilde{r}q} \varphi_{\beta\tilde{r}q}^{OBC}(\mathbf{r}) c_{\beta\tilde{r}\sigma q} \quad (20)$$

Using Eq. (5) we can define the 1D electron operators describing the slowly varying part of the electron operators $\Psi_{\beta\sigma}(\mathbf{r})$ as

$$\psi_{\beta\tilde{r}F\sigma}(u) = \frac{1}{\sqrt{2L}} \sum_q e^{i\text{sgn}(F)qu} c_{\beta\tilde{r}\sigma q}, \quad (21)$$

in terms of which the electron operators can be written as

$$\begin{aligned} \Psi_{\beta\sigma}(\mathbf{r}) &= \sum_{\tilde{r}q} \varphi_{\beta\tilde{r}q}^{OBC}(\mathbf{r}) c_{\beta\tilde{r}\sigma q} \\ &= \sqrt{L} \sum_{\tilde{r}F} \text{sgn}(F) \varphi_{\beta\text{sgn}(F)\tilde{r}F}(\mathbf{r}) \psi_{\beta\tilde{r}F\sigma}(u). \end{aligned} \quad (22)$$

For SWCNT shells with diameter larger than ~ 1 nm, we can only keep forward-scattering (or density-density) processes²⁰, such that the interacting Hamiltonian in an i-DWCNT becomes

$$H_{\text{i-DWCNT}}^{\text{int}} = \frac{1}{2} \sum_{\beta\beta'} \sum_{\tilde{r}\tilde{r}'} \sum_{FF'} \sum_{\sigma\sigma'} \iint du_1 du_2 \rho_{\beta\tilde{r}F\sigma}(u_1) V_{\beta\beta'}^{\text{eff}}(u_1 - u_2) \rho_{\beta'\tilde{r}'F'\sigma'}(u_2), \quad (23)$$

where $\rho_{\beta\tilde{r}F\sigma}(u) = \psi_{\beta\tilde{r}F\sigma}^\dagger(u) \psi_{\beta\tilde{r}F\sigma}(u)$ is the electron density operator and $V_{\beta\beta'}^{\text{eff}}$ is the effective one-dimensional Coulomb interactions given by

$$V_{\beta\beta'}^{\text{eff}}(u_1, u_2) = \frac{L^2}{N_\beta N_{\beta'}} \sum_{\mathbf{R}_1 \mathbf{R}_2} \iint dv_1 dv_2 |\chi(\mathbf{r}_1 - \mathbf{R}_1)|^2 U_{\beta\beta'}(\mathbf{r}_1 - \mathbf{r}_2) |\chi(\mathbf{r}_2 - \mathbf{R}_2)|^2. \quad (24)$$

Let us now turn to c-DWCNTs. The total Coulomb interaction Hamiltonian of a c-DWCNT has a similar form as Eq. (17). However, we have to rewrite it in the basis of the bonding/anti-bonding states using the transformation Eq. (14). In this basis, the Coulomb interaction of a c-DWCNT is given by

$$H_{\text{c-DWCNT}}^{\text{int}} = \frac{1}{2} \sum_{\nu\nu'\sigma\sigma'} \iint d\mathbf{r}_1 d\mathbf{r}_2 \Psi_{\nu\sigma}^\dagger(\mathbf{r}_1) \Psi_{\nu'\sigma'}^\dagger(\mathbf{r}_2) \tilde{U}_{\nu\nu'}(\mathbf{r}_1 - \mathbf{r}_2) \Psi_{\nu'\sigma'}(\mathbf{r}_2) \Psi_{\nu\sigma}(\mathbf{r}_1), \quad (25)$$

where $\nu = \pm$ is the index for bonding and anti-bonding bands and the new interactions are

$$\tilde{U}_{+-} = 2\tilde{U}_{++} = 2\tilde{U}_{--} = \frac{1}{4}(U_{++} + U_{--} + U_{+-}), \quad (26)$$

where $U_{\beta\beta'}$ is defined by Eqs. (18) and (19). The electron operators in c-DWCNTs are defined as

$$\begin{aligned} \Psi_{\nu\sigma}(\mathbf{r}) &= \sum_{\tilde{r}q} \tilde{\varphi}_{\nu\tilde{r}q}^{OBC}(\mathbf{r}) \tilde{c}_{\nu\tilde{r}\sigma q} \\ &= \sqrt{L} \sum_{\tilde{r}F} \text{sgn}(F) \tilde{\varphi}_{\nu\text{sgn}(F)\tilde{r}F}(\mathbf{r}) \tilde{\psi}_{\nu\tilde{r}\sigma F}(u), \end{aligned} \quad (27)$$

where $\tilde{\varphi}_{\nu\tilde{r}q}^{OBC}$ is a linear combination of $\varphi_{\beta\tilde{r}q}^{OBC}$, namely, $\tilde{\varphi}_{\nu\tilde{r}q}^{OBC}(\mathbf{r}) = ((\varphi_{+\tilde{r}q}^{OBC}(\mathbf{r}) + \text{sgn}(\nu)\varphi_{-\tilde{r}q}^{OBC}(\mathbf{r}))/\sqrt{2})$. By using these electron operators and keeping only the relevant forward-scattering processes, the Coulomb interaction Hamiltonian of a c-DWCNT becomes

$$H_{\text{c-DWCNT}}^{\text{int}} = \frac{1}{2} \sum_{\nu\nu'} \sum_{\tilde{r}\tilde{r}'} \sum_{FF'} \sum_{\sigma\sigma'} \iint du_1 du_2 \tilde{\rho}_{\nu\tilde{r}F\sigma}(u_1) \tilde{V}_{\nu\nu'}^{\text{eff}}(u_1 - u_2) \tilde{\rho}_{\nu'\tilde{r}'F'\sigma'}(u_2), \quad (28)$$

where $\tilde{\rho}_{\nu\tilde{r}F\sigma}(u) = \tilde{\psi}_{\nu\tilde{r}F\sigma}^\dagger(u) \tilde{\psi}_{\nu\tilde{r}F\sigma}(u)$ is the density operator and $\tilde{V}_{\nu\nu'}^{\text{eff}}$ is the effective one-dimensional Coulomb interaction,

$$\tilde{V}_{\nu\nu'}^{\text{eff}}(u_1, u_2) = \frac{L^2}{N_\nu N_{\nu'}} \sum_{\mathbf{R}_1 \mathbf{R}_2} \iint dv_1 dv_2 |\chi(\mathbf{r}_1 - \mathbf{R}_1)|^2 \tilde{U}_{\nu\nu'}(\mathbf{r}_1 - \mathbf{r}_2) |\chi(\mathbf{r}_2 - \mathbf{R}_2)|^2. \quad (29)$$

C. Bosonization

The low energy Hamiltonian of a DWCNT is the combination of the non-interacting and interacting Hamiltonians and it can be diagonalized by the bosonization method^{30,31,32,33}. First, we introduce the bosonic operators^{19,25,32}

$$b_{\alpha\text{sgn}(\tilde{r})q\sigma} = \begin{cases} \rho_{\alpha\tilde{r}q\sigma} / \sqrt{n_q}, & \text{for i-DWCNTs,} \\ \tilde{\rho}_{\alpha\tilde{r}q\sigma} / \sqrt{n_q}, & \text{for c-DWCNTs,} \end{cases} \quad (30)$$

where $q = \pi n_q / L$ with n_q an integer. The index $\alpha = \pm$ denotes the bonding/anti-bonding states in c-DWCNTs and outer/inner shells in i-DWCNTs and we will keep this convention in the rest of the paper. The bosonic operators obey the bosonic commutation relation

$$[b_{\alpha q\sigma}, b_{\alpha'q'\sigma'}^\dagger] = \delta_{\alpha\alpha'} \delta_{qq'} \delta_{\sigma\sigma'}.$$

By using these bosonic operators, the Hamiltonian of a DWCNT QD can be separated into its fermionic and bosonic parts, $H_{QD} = H_f + H_b$. The fermionic part H_f describes the ground state and the fermionic excitations in the DWCNT. The fermionic Hamiltonian of a c-DWCNT is

$$H_{f,\text{c-DWCNT}} = \sum_{\alpha\tilde{r}\sigma} \frac{1}{2} \varepsilon_0 \mathcal{N}_{\alpha\tilde{r}\sigma}^2 + \Delta \varepsilon_0 \text{sgn}(\tilde{r}) \mathcal{N}_{\alpha\tilde{r}\sigma} + \left(\alpha \zeta \varepsilon_0 - \frac{1}{2} \varepsilon_0 \right) \mathcal{N}_{\alpha\tilde{r}\sigma} + H_f^{\text{int}}, \quad (31)$$

while the i-DWCNT fermionic Hamiltonian has the form

$$H_{f,\text{i-DWCNT}} = \sum_{\alpha\tilde{r}\sigma} \frac{1}{2} \varepsilon_0 \mathcal{N}_{\alpha\tilde{r}\sigma}^2 + \Delta_\alpha \varepsilon_0 \text{sgn}(\tilde{r}) \mathcal{N}_{\alpha\tilde{r}\sigma} - \frac{1}{2} \varepsilon_0 \mathcal{N}_{\alpha\tilde{r}\sigma} + H_f^{\text{int}}, \quad (32)$$

where H_f^{int} is due to Coulomb interaction having the form

$$H_f^{\text{int}} = \frac{1}{2} \sum_{\alpha\alpha'} W_{00}^{\alpha\alpha'} \left(\sum_{\tilde{r}\sigma} \mathcal{N}_{\alpha\tilde{r}\sigma} \right) \left(\sum_{\tilde{r}'\sigma'} \mathcal{N}_{\alpha'\tilde{r}'\sigma'} \right), \quad (33)$$

with the interaction strengths

$$W_{00}^{\alpha\alpha'} = \frac{1}{L^2} \iint du_1 du_2 V_{\alpha\alpha'}^{\text{eff}}(u_1 - u_2).$$

Therefore, the fermionic Hamiltonian of a DWCNT QD is described by the constant-interaction model¹⁴.

The bosonic excitations of a DWCNT QD are described by the Hamiltonian H_b , which can be expressed in terms of the bosonic operators as

$$H_b = \sum_{q \neq 0} \sum_{\alpha\sigma\tilde{r}} \varepsilon_0 |n_q| b_{\alpha\text{sgn}(\tilde{r})q\sigma}^\dagger b_{\alpha\text{sgn}(\tilde{r})q\sigma} + \frac{1}{2} \sum_{q > 0} \sum_{\alpha\alpha'\tilde{r}\tilde{r}'\sigma\sigma'} n_q W_{qq}^{\alpha\alpha'} (b_{\alpha\text{sgn}(\tilde{r})q\sigma} + b_{\alpha\text{sgn}(\tilde{r})q\sigma}^\dagger) (b_{\alpha'\text{sgn}(\tilde{r}')q\sigma'} + b_{\alpha'\text{sgn}(\tilde{r}')q\sigma'}^\dagger), \quad (34)$$

with the interaction strengths

$$W_{qq}^{\alpha\alpha'} = \frac{1}{L^2} \iint du_1 du_2 V_{\alpha\alpha'}^{eff}(u_1 - u_2) \cos(qu_1) \cos(qu_2). \quad (35)$$

In order to diagonalize the Hamiltonian H_b , we need to introduce new bosonic operators $a_{j\delta\xi q}$'s, where $j = c, s$ denote charge/spin modes and the remaining indices $\delta = \pm$ and $\xi = \pm$ define total/relative modes with respect to the branch and shell (or bonding/anti-bonding state) degrees of freedoms, respectively. The new bosonic operators are related to the bosonic operators $b_{\alpha\text{sgn}(\bar{r})q\sigma}$'s as^{25,34}

$$b_{\alpha\text{sgn}(\bar{r})q\sigma} = \sum_{j\delta\xi} \Lambda_{\alpha\bar{r}\sigma}^{j\delta\xi q} (S_{j\delta\xi q} a_{j\delta\xi q} + C_{j\delta\xi q} a_{j\delta\xi q}^\dagger), \quad (36)$$

where the coefficients are given by

$$\Lambda_{\alpha\bar{r}\sigma}^{j\delta\xi q} = \frac{1}{2\sqrt{2}} \begin{pmatrix} \sin\theta_q + \cos\theta_q & -\cos\theta_q + \sin\theta_q & 1 & 1 & 1 & 1 & 1 & 1 \\ \sin\theta_q + \cos\theta_q & -\cos\theta_q + \sin\theta_q & 1 & 1 & -1 & -1 & -1 & -1 \\ \sin\theta_q + \cos\theta_q & -\cos\theta_q + \sin\theta_q & -1 & -1 & 1 & 1 & -1 & -1 \\ \sin\theta_q + \cos\theta_q & -\cos\theta_q + \sin\theta_q & -1 & -1 & -1 & -1 & 1 & 1 \\ \sin\theta_q + \cos\theta_q & -\cos\theta_q - \sin\theta_q & 1 & -1 & 1 & -1 & 1 & -1 \\ \sin\theta_q + \cos\theta_q & -\cos\theta_q - \sin\theta_q & 1 & -1 & -1 & 1 & -1 & 1 \\ \sin\theta_q + \cos\theta_q & -\cos\theta_q - \sin\theta_q & -1 & 1 & 1 & -1 & -1 & 1 \\ \sin\theta_q + \cos\theta_q & -\cos\theta_q - \sin\theta_q & -1 & 1 & -1 & 1 & 1 & -1 \end{pmatrix}, \quad (37)$$

with

$$\sin\theta_q = \left| W_{qq}^{++} - W_{qq}^{--} \right| / \left(\left(W_{qq}^{++} - W_{qq}^{--} \right)^2 + \left(W_{qq}^{+-} + \sqrt{\left(W_{qq}^{++} - W_{qq}^{--} \right)^2 + \left(W_{qq}^{+-} \right)^2} \right)^2 \right)^{1/2}.$$

The other coefficients are

$$S_{j\delta\xi q} = 1 \quad \text{and} \quad C_{j\delta\xi q} = 0 \quad (38)$$

in the cases $(j\delta\xi) = (c-\pm), (s\pm\pm)$. For the total and relative charge modes $(c+\pm)$, the two coefficients are interaction dependent

$$S_{c+\pm q} = \frac{1}{2} \left(\sqrt{\frac{\varepsilon_0}{\varepsilon_{c+\pm}(q)}} + \sqrt{\frac{\varepsilon_{c+\pm}(q)}{\varepsilon_0}} \right), \quad C_{c+\pm q} = \frac{1}{2} \left(\sqrt{\frac{\varepsilon_0}{\varepsilon_{c+\pm}(q)}} - \sqrt{\frac{\varepsilon_{c+\pm}(q)}{\varepsilon_0}} \right), \quad (39)$$

where the energies of the total and relative charge modes are

$$\varepsilon_{c+\pm}(q) = \varepsilon_0 \sqrt{1 + 8W_{qq}^{\pm\pm}/\varepsilon_0}. \quad (40)$$

The interactions do not affect the 6 ‘‘neutral’’ modes, $(j\delta\xi) = (c-\pm), (s\pm\pm)$ and their energy dispersions are the same as for the non-interacting system,

$$\varepsilon_{j\delta\xi}(q) = \varepsilon_0. \quad (41)$$

By using the new bosonic operators, the excitation Hamiltonian can be diagonalized to be

$$H_b = \sum_{q>0} \sum_{j\delta\xi} \varepsilon_{j\delta\xi}(q) a_{j\delta\xi q}^\dagger a_{j\delta\xi q}, \quad (42)$$

and the eigenstates are

$$|\mathbf{N}, \mathbf{m}\rangle \equiv \prod_{q>0} \prod_{j\delta\xi} \frac{1}{\sqrt{m_{j\delta\xi q}!}} \left(a_{j\delta\xi q}^\dagger \right)^{m_{j\delta\xi q}} |\mathbf{N}, \mathbf{0}\rangle, \quad (43)$$

where $\mathbf{N} = \{N_{\alpha\bar{r}\sigma}\}$ defines the number of electrons in each of the eight branches $(\alpha\bar{r}\sigma)$ and $\mathbf{m} = \{m_{j\delta\xi q}\}$ describes the configuration of the bosonic excitations in each of the eight modes $(j\delta\xi)$. The state $|\mathbf{N}, \mathbf{0}\rangle$ contains no bosonic excitations and describes the ground state or the fermionic excited states.

III. DYNAMICS OF THE QD SYSTEM

The transport properties of the DWCNT QD system can be obtained by investigating the dynamics of its density matrix³⁵. In this section, we briefly show how to derive the equation of motion for the reduced density matrix of the DWCNT QD system. By solving these equations we obtain the stationary current through the DWCNT QD system when a bias voltage is applied.

A. Equation of motion for the reduced density matrix

As we consider a very weak coupling between the DWCNT QD and the two leads, the tunneling Hamiltonian can be treated as a perturbation and we can obtain the equation for motion for the density matrix in the interaction picture as³⁵

$$i\hbar \frac{\partial \rho_{tot}^I(t)}{\partial t} = [H_T^I(t), \rho_{tot}^I(t)], \quad (44)$$

where $\rho_{tot}^I(t)$ is the density matrix of the whole system (including the DWCNT QD and the leads) and the tunneling Hamiltonian in the interaction picture is

$$H_T^I(t) = e^{\frac{i}{\hbar}(H_{QD}+H_{leads})(t-t_0)} H_T e^{-\frac{i}{\hbar}(H_{QD}+H_{leads})(t-t_0)}. \quad (45)$$

This equation can be solved formally as

$$\rho_{tot}^I(t) = \rho_{tot}^I(t_0) - \frac{i}{\hbar} \int_{t_0}^t dt_1 [H_T^I(t_1), \rho_{tot}^I(t_1)]. \quad (46)$$

Substituting the above expression of $\rho_{tot}^I(t)$ back to Eq. (44), we have

$$\frac{\partial \rho_{tot}^I(t)}{\partial t} = -\frac{i}{\hbar} [H_T^I(t), \rho_{tot}^I(t_0)] + \left(\frac{i}{\hbar}\right)^2 \int_{t_0}^t dt_1 [H_T^I(t), [H_T^I(t_1), \rho_{tot}^I(t_1)]]. \quad (47)$$

As we are only interested in the transport through the DWCNT QD, we will focus on the reduced density matrix of the QD which is obtained by tracing out the degrees of freedom of the leads,

$$\rho^I = \text{Tr}_{\text{leads}}\{\rho_{tot}^I\}. \quad (48)$$

Because the leads are very large comparing with the QD and the tunneling events between leads and the QD are rare, the effect of the QD on the leads can be ignored and the leads can be described as reservoirs remaining in thermal equilibrium. We use the ansatz¹⁹ to factorize the total density matrix $\rho^I(t)$,

$$\rho_{tot}^I(t) = \rho_{\text{leads}}^I \rho^I(t) = \rho_s^I \rho_d^I \rho^I(t), \quad (49)$$

where the density matrix of the leads, ρ_{leads} , is time independent and is described by the thermal equilibrium distribution,

$$\rho_{s/d}^I = \frac{e^{-\beta(H_{s/d} - \mu_{s/d} \mathcal{N}_{s/d})}}{\text{Tr}\{e^{-\beta(H_{s/d} - \mu_{s/d} \mathcal{N}_{s/d})}\}},$$

where $\mu_{s/d}$ is the chemical potential of the source/drain lead and $\beta = 1/k_B T$. We further simplify Eq. (47) by introducing the Markov approximation, that is, we assume that $\dot{\rho}_{tot}^I(t)$ only locally depends on $\rho_{tot}^I(t)$ and we can replace $\rho_{tot}^I(t')$ by $\rho_{tot}^I(t)$.

We make the further assumptions that the elements of the reduced density matrix between two states with different charges vanish, and that the elements between two non-degenerate states with same charges also vanish^{18,19}. Finally, the master equations of the reduced density matrix can be expressed in Bloch-Redfield form^{36,37}

$$\dot{\rho}_{nm}^{I,E_N}(t) = - \sum_{kk'} R_{nmkk'}^{E_N} \rho_{kk'}^{I,E_N}(t) + \sum_{M=N\pm 1} \sum_{E'} \sum_{kk'} R_{nmkk'}^{E_N E'} \rho_{kk'}^{I,E'M}(t), \quad (50)$$

where n, m, k , and k' are indices of the eigenstates of the DWCNT QD Hamiltonian. The Redfield tensors have the form

$$R_{nm\,kk'}^{E_N} = \sum_l \sum_{M, E', j} \left(\delta_{mk'} \Gamma_{l, njjk}^{(+), E_N, E'_M} + \delta_{nk} \Gamma_{l, k' jjm}^{(-), E_N, E'_M} \right), \quad (51)$$

$$R_{nm\,kk'}^{E_N, E'_M} = \sum_l \Gamma_{l k' mnk}^{(+), E'_M, E_N} + \Gamma_{l k' mnk}^{(-), E'_M, E_N}, \quad (52)$$

and the matrix elements of the electron operators are

$$\left(\Psi_{\alpha\sigma}^\dagger(\mathbf{x}) \right)_{km}^{E_N, E'_{N+1}} = \langle \mathbf{N}, \mathbf{k} | \Psi_{\alpha\sigma}^\dagger(\mathbf{x}) | \mathbf{N} + \mathbf{1}, \mathbf{m} \rangle$$

with the states $|\mathbf{N}, \mathbf{k}\rangle$ and $|\mathbf{N} + \mathbf{1}, \mathbf{m}\rangle$ having energy E_N, E'_{N+1} and particle number $N, N + 1$, respectively. Such matrix elements are calculated in analytic form in App. A. The transition rates depend on the properties of the contacts between the leads and the DWCNT QD¹⁹. Here, we assume that the contacts are very simple. They do not mix the electrons in the different branches and the couplings between the leads and the DWCNT do not depend on either the wave vectors or the spins of the tunneling electrons. Then the transition rates depend on the energy of the tunneling electrons because of the matrix elements of the electron operators, Eq. (A3) and have the forms (the derivation of these expressions is given in App. B),

$$\begin{aligned} \Gamma_{lk'mnk}^{(\pm), E_N, E_{N+1}} &= \sum_{\alpha} \frac{\gamma_{l\alpha}}{\hbar} g_l(\varepsilon_l) f(\varepsilon_l) \sum_{\tilde{r}\sigma F} \delta_{\mathbf{N} + \mathbf{e}_{\alpha\tilde{r}\sigma}, \mathbf{N} + \mathbf{1}} \prod_{q>0} \prod_{q'>0} \prod_{j\delta\xi} \prod_{j'\delta'\xi'} \\ &\times F(\lambda_{\alpha\tilde{r}\sigma q}^{j\delta\xi F}(u_l), k'_{j\delta\xi q}, m_{j\delta\xi q}) F^*(\lambda_{\alpha\tilde{r}\sigma q}^{j'\delta'\xi' F}(u_l), n_{j'\delta'\xi' q'}, k_{j'\delta'\xi' q'}) \end{aligned} \quad (53)$$

where the constants $\gamma_{l\alpha}$ describes the coupling strengths between the bonding/anti-bonding state α in c-DWCNTs or between the shell α in i-DWCNTs and the leads l and $u_l = 0, L$ for $l = s, d$. The vector $\mathbf{e}_{\alpha\tilde{r}\sigma}$ denotes a state with one particle in the branch $\alpha\tilde{r}\sigma$. The function $F(\lambda, m, m')$ is defined in Eq. (A4) and the parameters $\lambda_{\alpha\tilde{r}\sigma q}^{j\delta\xi F}(u)$'s are defined in Eq. (A5). The eigenstates involved are

$$\begin{aligned} |k'\rangle &= |\mathbf{N}, \mathbf{k}'\rangle, & |m\rangle &= |\mathbf{N} + \mathbf{1}, \mathbf{m}\rangle, \\ |n\rangle &= |\mathbf{N} + \mathbf{1}, \mathbf{n}\rangle, & |k\rangle &= |\mathbf{N}, \mathbf{k}\rangle. \end{aligned}$$

Similarly, the expressions for the remaining tunneling rates are

$$\begin{aligned} \Gamma_{lk'mnk}^{(\pm), E_N, E_{N-1}} &= \sum_{\alpha} \frac{\gamma_{l\alpha}}{\hbar} g_l(\varepsilon_l) (1 - f(\varepsilon_l)) \sum_{\tilde{r}\sigma F} \delta_{\mathbf{N} - \mathbf{e}_{\alpha\tilde{r}\sigma}, \mathbf{N} - \mathbf{1}} \prod_{q>0} \prod_{q'>0} \prod_{j\delta\xi} \prod_{j'\delta'\xi'} \\ &\times F^*(\lambda_{\alpha\tilde{r}\sigma q}^{j\delta\xi F}(u_l), k'_{j\delta\xi q}, m_{j\delta\xi q}) F(\lambda_{\alpha\tilde{r}\sigma q}^{j'\delta'\xi' F}(u_l), n_{j'\delta'\xi' q'}, k_{j'\delta'\xi' q'}) \end{aligned} \quad (54)$$

with the eigenstates

$$\begin{aligned} |k'\rangle &= |\mathbf{N}, \mathbf{k}'\rangle, & |m\rangle &= |\mathbf{N} - \mathbf{1}, \mathbf{m}\rangle, \\ |n\rangle &= |\mathbf{N} - \mathbf{1}, \mathbf{n}\rangle, & |k\rangle &= |\mathbf{N}, \mathbf{k}\rangle. \end{aligned}$$

In the linear transport regime, only the following tunneling rates between the ground states with N and $N \pm 1$ electrons are needed, which have very simple expressions,

$$\Gamma_{lknnk}^{(\pm), E_N, E_{N+1}} = \sum_{\alpha} \sum_{\tilde{r}\sigma F} \frac{\gamma_{l\alpha}}{\hbar} g_l(\varepsilon_l) f(\varepsilon_l) \delta_{\mathbf{N} + \mathbf{e}_{\alpha\tilde{r}\sigma}, \mathbf{N} + \mathbf{1}} \quad (55)$$

with the eigenstates $|k\rangle = |\mathbf{N}, \mathbf{0}\rangle$ and $|n\rangle = |\mathbf{N} + \mathbf{1}, \mathbf{0}\rangle$, and

$$\Gamma_{lknnk}^{(\pm), E_N, E_{N-1}} = \sum_{\alpha} \sum_{\tilde{r}\sigma F} \frac{\gamma_{l\alpha}}{\hbar} g_l(\varepsilon_l) (1 - f(\varepsilon_l)) \delta_{\mathbf{N} - \mathbf{e}_{\alpha\tilde{r}\sigma}, \mathbf{N} - \mathbf{1}} \quad (56)$$

with the eigenstates $|k\rangle = |\mathbf{N}, \mathbf{0}\rangle$ and $|n\rangle = |\mathbf{N} - \mathbf{1}, \mathbf{0}\rangle$. We are only interested in the properties of the system in the stationary state, which can be obtained by solving the Eq. (50) with the left hand side set to be zero.

B. Calculation of the current

The current can be calculated by using the tunneling rates between the DWCNT QD and the leads. The current measured in experiments is the current in one lead, which can be calculated as

$$I_l = e \sum_N (\Theta_l^{N \rightarrow N+1} - \Theta_l^{N \rightarrow N-1}), \quad (57)$$

where $\Theta_l^{N \rightarrow N \pm 1}$ are the tunneling rates between the QD and the lead l when the particle number in the DWCNT QD changes from N to $N \pm 1$. The tunneling rates are related to the transition rates and the reduced density matrix as

$$\Theta_l^{N \rightarrow N \pm 1} = \sum_{E, E'} \sum_{nkj} \left(\Gamma_{l, njjk}^{(+), E_N, E'_{N \pm 1}} \rho_{kn}^{I, E_N} + \rho_{nk}^{I, E_N} \Gamma_{l, kjjn}^{(-), E_N, E'_{N \pm 1}} \right). \quad (58)$$

After substituting Eq. (58) into Eq. (57), the current can be expressed in terms of the transition rates and the elements of the reduced density matrix as

$$I_l = e \sum_{N, E, E'} \left(\Gamma_{l, njjk}^{(+), E_N, E'_{N+1}} - \Gamma_{l, njjk}^{(+), E_N, E'_{N-1}} \right) \rho_{kn}^{I, E_N} + \left(\Gamma_{l, kjjn}^{(-), E_N, E'_{N+1}} - \Gamma_{l, kjjn}^{(-), E_N, E'_{N-1}} \right) \rho_{nk}^{I, E_N}. \quad (59)$$

IV. LINEAR AND NONLINEAR TRANSPORT

After having obtained the energy spectrum and the eigenstates of the DWCNT QD system, we can calculate the transition rates, Eqs. (53) and (54) and use the Bloch-Redfield equations for the reduced density matrix to calculate the transport properties of the system. Here we present the calculated results of both linear and nonlinear conductances.

A. Linear conductance

In the linear transport regime, i.e., $|eV_b| \ll k_B T \ll \varepsilon_0$, where V_b is the applied bias, only the ground states with N and $N + 1$ electrons are involved in the transport. In this case, the equations for the diagonal elements and the off-diagonal elements of the reduced density matrix are decoupled from each other and we only have to take into account the diagonal elements of the ground states with a certain electron number, which are the occupation probabilities. The stationary occupation probability of the ground state with N electrons is given as¹⁹

$$P_N = \frac{\sum_{l\alpha} \gamma_{l\alpha} (1 - f(\varepsilon_l)) C_{N+1, N}^\alpha}{\sum_{l\alpha} \gamma_{l\alpha} f(\varepsilon_l) C_{N, N+1}^\alpha + \sum_{l\alpha} \gamma_{l\alpha} (1 - f(\varepsilon_l)) C_{N+1, N}^\alpha}, \quad (60)$$

where $C_{N, N+1}^\alpha$ are the number of permitted ground states with $N + 1$ particles when one electron is added to a ground state with N particles and this electron is added to the bonding/anti-bonding state α in c-DWCNTs or to the shell α in i-DWCNTs. We define the energy $\varepsilon_l = eV_l - \Delta E$ and the energy difference $\Delta E = E_N^0 - E_{N+1}^0 - \mu_g$, where μ_g is the electrochemical potential in the gate. The linear conductance is then given as

$$G = \frac{2e^2\beta}{h} \frac{\sum_{\alpha} \gamma_{s\alpha} \gamma_{d\alpha} C_{N, N+1}^\alpha C_{N+1, N}^\alpha}{\sum_{l\alpha} \gamma_{l\alpha} f(-\Delta E) C_{N, N+1}^\alpha + \sum_{l\alpha} \gamma_{l\alpha} (1 - f(-\Delta E)) C_{N+1, N}^\alpha} \frac{e^{-\beta\Delta E}}{(1 + e^{-\beta\Delta E})^2}, \quad (61)$$

where we assume that the bias is symmetrically applied to the source and drain leads, that is, $-V_s = V_d = V_b/2$. The maximum value of the linear conductance is

$$G_{\max} = \frac{2e^2\beta}{h} \frac{\sum_{\alpha} \gamma_{s\alpha} \gamma_{d\alpha} C_{N, N+1}^\alpha C_{N+1, N}^\alpha}{\sum_{l\alpha} \gamma_{l\alpha} (C_{N, N+1}^\alpha + C_{N+1, N}^\alpha) + 2\sqrt{(\sum_{l\alpha} \gamma_{l\alpha} C_{N, N+1}^\alpha)(\sum_{l\alpha} \gamma_{l\alpha} C_{N+1, N}^\alpha)}}. \quad (62)$$

and the maxima of the conductance as a function of μ_g are at $-\mu_g = E_{N+1}^0 - E_N^0 + \Delta E_{\max}$, where^{15,18,19,38,39}

$$\Delta E_{\max} = \frac{1}{2\beta} \ln \frac{\sum_{l\alpha} \gamma_{l\alpha} C_{N+1, N}^\alpha}{\sum_{l\alpha} \gamma_{l\alpha} C_{N, N+1}^\alpha}. \quad (63)$$

The conductance peak occurs whenever an electron is added or removed from the DWCNT QD by changing the electrochemical potential in the gate. At zero temperature, from Eq. (63) ΔE_{\max} vanishes and the conductance peak occurs when the electrochemical potential of the gate satisfies the following condition,

$$-\mu_g = E_{N+1}^0 - E_N^0 \equiv \mu_N.$$

Therefore, at zero temperature the addition energy $\delta\mu_N$ is given by

$$\delta\mu_N = |\mu_N - \mu_{N-1}| = |E_{N+1}^0 + E_{N-1}^0 - 2E_N^0|.$$

For a c-DWCNT QD system, electrons can tunnel into both shells because of nonzero intershell couplings. Hence there is an 8-electron periodicity of the conductance peak distances, which are

$$\delta\mu_1 = \delta\mu_3 = \delta\mu_5 = \delta\mu_7 = W_{00}^{++}, \quad (64)$$

$$\delta\mu_2 = \mu_6 = 2 \min(\Delta, \zeta)\varepsilon_0 + W_{00}^{++}, \quad (65)$$

$$\delta\mu_4 = 2|\Delta - \zeta|\varepsilon_0 + W_{00}^{++}, \quad (66)$$

$$\delta\mu_8 = \varepsilon_0 - 2(\Delta + \zeta)\varepsilon_0 + W_{00}^{++}. \quad (67)$$

Here, we use the relation, $W_{00}^{++} = W_{00}^{--} = W_{00}^{+-}/2$, in c-DWCNTs (cf. Eq. (26)). On the other hand, electrons can only tunnel into the outer shell in an i-DWCNT QD system because the contacts are deposited onto the outer shell and the intershell couplings vanish. Therefore, there is a 4-electron periodicity of the conductance peak distance like in a SWCNT QD system, which are

$$\delta\mu_1 = \delta\mu_3 = W_{00}^{++}, \quad (68)$$

$$\delta\mu_2 = 2\Delta_+\varepsilon_0 + W_{00}^{++}, \quad (69)$$

$$\delta\mu_4 = \varepsilon_0 - 2\Delta_+\varepsilon_0 + W_{00}^{++}. \quad (70)$$

Because electrons tunnel only into the outer shell with the interaction strength W_{00}^{++} , the addition energy $\delta\mu_N$ does not depend either on the interaction strength in the inner shell W_{00}^{--} nor on the intrashell interaction strength W_{00}^{+-} . The calculated linear conductances of DWCNT QDs of different configurations are shown in Figs. 5 and 6. In a c-DWCNT QD, the intraband interaction strengths W_{00}^{++} and W_{00}^{--} are the same while the interband interaction strength W_{00}^{+-} is twice as large (cf. Eq. (26)). However, in an i-DWCNT the interaction strength in the inner shell W_{00}^{--} is the strongest because of the smaller inner shell radius and one has $W_{00}^{--} > W_{00}^{+-} > W_{00}^{++}$. The shapes of the conductance peaks strongly depend on the mismatch parameters, i.e., Δ and ζ in c-DWCNTs and Δ_{\pm} in i-DWCNTs. For zero mismatch parameters, the quantities $C_{N,N+1}^{\alpha}$ and $C_{N+1,N}^{\alpha}$ are $C_{N,N+1}^{\alpha} = 4, 3, 2, 1$ and $C_{N+1,N}^{\alpha} = 1, 2, 3, 4$ for $N^{\alpha} = 4m, 4m+1, 4m+2, 4m+3$ with an integer m , where N^{α} is the electron number either in the bonding/anti-bonding state α in c-DWCNTs or in the shell α in i-DWCNTs. Therefore, according to Eq. (62) one can find that the conductance peak heights show an 8-electron periodicity in a c-DWCNT QD (cf. Fig. 5(a)) because both bonding and anti-bonding states contribute to the electron transport. However, there is a 4-electron periodicity in an i-DWCNT QD (cf. Fig. 6(a)) because only the outer shell contributes. If the mismatch parameters are nonzero, we find $C_{N,N+1}^{\alpha} = 2, 1, 2, 1$ and $C_{N+1,N}^{\alpha} = 1, 2, 1, 2$ for $N^{\alpha} = 4m, 4m+1, 4m+2, 4m+3$. Therefore, all the conductance peaks have the same heights (cf. Fig. 5(b) and 6(b)). However, the distance between two conductance peaks, i.e., the addition energy, always shows an 8-electron periodicity in c-DWCNT QDs and the 4-electron periodicity in i-DWCNTs as shown in the Figs. 5 and 6.

B. Nonlinear conductances

When higher bias is applied, i.e., $|eV_b| \geq \varepsilon_0 \gg k_B T$, we can only solve the Bloch-Redfield equations numerically. For elastic tunneling process, we have to include the coherences between the states with same particle number \mathbf{N} but with different bosonic excitations \mathbf{m} ^{18,19}. Because of the large number of degenerate bosonic excitations, the rank of the reduced density matrix increases very fast as the applied bias increases, which causes a very long computing time to solve the equations. On the other hand, these coherences can be ignored in an inelastic tunneling process, in which the QD system will be restored to the equilibrium states before the next tunneling process. Only the diagonal elements in the reduced density matrix are nonzero and they obey the Boltzmann distribution as

$$\rho_{nn}^{I,E_N}(t) = \mathcal{P}_N(t) \frac{e^{-\beta E_N^n}}{\sum_k e^{-\beta E_N^k}},$$

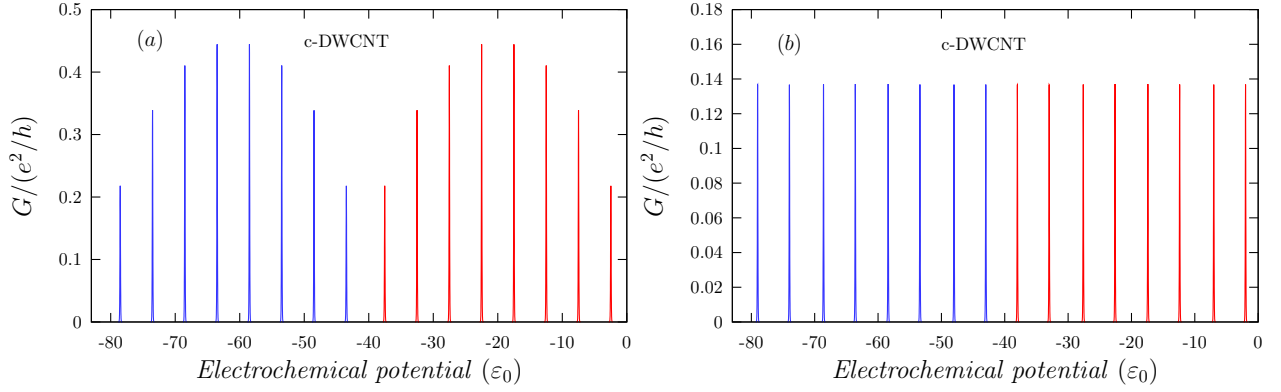


FIG. 5: (Color online) Calculated linear conductances as a function of the gate electrochemical potential in commensurate double-walled carbon nanotube (c-DWCNT) quantum dot (QD) systems with different parameters. (a): $\Delta = \zeta = 0.0$, $W_{00}^{++} = W_{00}^{--} = W_{00}^{+-}/2 = 5.0\epsilon_0$, and $k_B T = 0.025\epsilon_0$, where the level spacing ϵ_0 is used as the unit of energy. The coupling strengths are $\gamma_{s\pm} = \gamma_{d\pm} = 0.01\epsilon_0$. (b): $\Delta = 0.2$ and $\zeta = 0.3$. The remaining parameters are the same as those in (a). In both cases, the linear conductances in c-DWCNTs show an 8-electron periodicity. In the case of zero mismatch parameters shown in (a), an 8-electron periodicity of the heights of the conductance peaks also occurs. For finite mismatch shown in (b), the peak heights are equal but the 8-electron periodicity of the addition energies, i.e., the peak distances, remains, (to emphasize this we assign to each ground of eight peaks different colors).

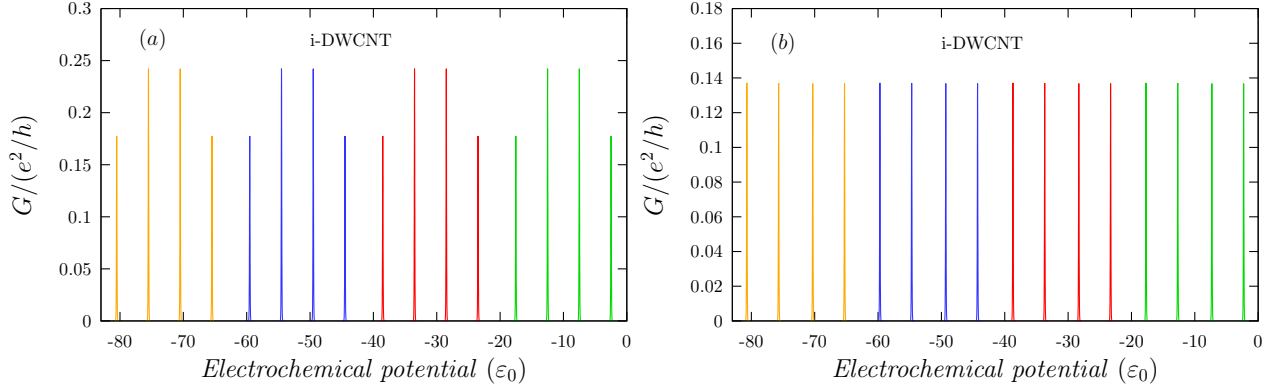


FIG. 6: (Color online) Calculated linear conductances as a function of the gate electrochemical potential in incommensurate double-walled carbon nanotube (i-DWCNT) quantum dot (QD) systems with different parameters. (a) $\Delta_+ = \Delta_- = 0.0$, $W_{00}^{++} = 5\epsilon_0$, $W_{00}^{--} = 6.0\epsilon_0$, $W_{00}^{+-} = 5.5\epsilon_0$, and $k_B T = 0.025\epsilon_0$, where the level spacing ϵ_0 is used as the unit of energy. The coupling strengths are $\gamma_{s+} = \gamma_{d+} = 0.01\epsilon_0$ and $\gamma_{s-} = \gamma_{d-} = 0$. (b): $\Delta_+ = 0.2$ and $\Delta_- = 0.3$. The remaining parameters are the same as those in (a). The linear conductances in i-DWCNTs show a 4-electron periodicity. In the absence of mismatch shown in (a), the 4-electron periodicity is observed also in the peak heights while it is no longer observed at finite mismatch shown in (b). However, the addition energy, i.e., the peak distance, shows a 4-electron periodicity in both cases, (to emphasize this we assign to each ground of eight peaks different colors).

where n and k are indices of the eigenstates of the DWCNT QD Hamiltonian and $\mathcal{P}_N(t)$ is the probability of finding N electrons in the QD. Instead of solving the Bloch-Redfield equations directly, we can solve the equation of motion for the probability $\mathcal{P}_N(t)$,

$$\frac{d}{dt}\mathcal{P}_N(t) = - \sum_{l,M=N\pm 1} \Theta_l^{N\rightarrow M} + \sum_{l,M=N\pm 1} \Theta_l^{M\rightarrow N}, \quad (71)$$

where the tunneling rate is defined in Eq. (58) and can now be expressed in terms of $\mathcal{P}_N(t)$ as

$$\Theta_l^{N\rightarrow N\pm 1} = \mathcal{P}_N(t) \sum_{E,E'} \frac{e^{-\beta E_N^n}}{\sum_k e^{-\beta E_N^k}} \left(\sum_{nj} \Gamma_{l,njjn}^{(+)} E_N E'_{N\pm 1} + \Gamma_{l,njjn}^{(-)} E_N E'_{N\pm 1} \right). \quad (72)$$

The number of the equations reduces significantly and the equations can be solved quite fast. In Fig. 7, we show the calculated stability diagram of a DWCNT QD system in an inelastic tunneling process. The size of the Coulomb

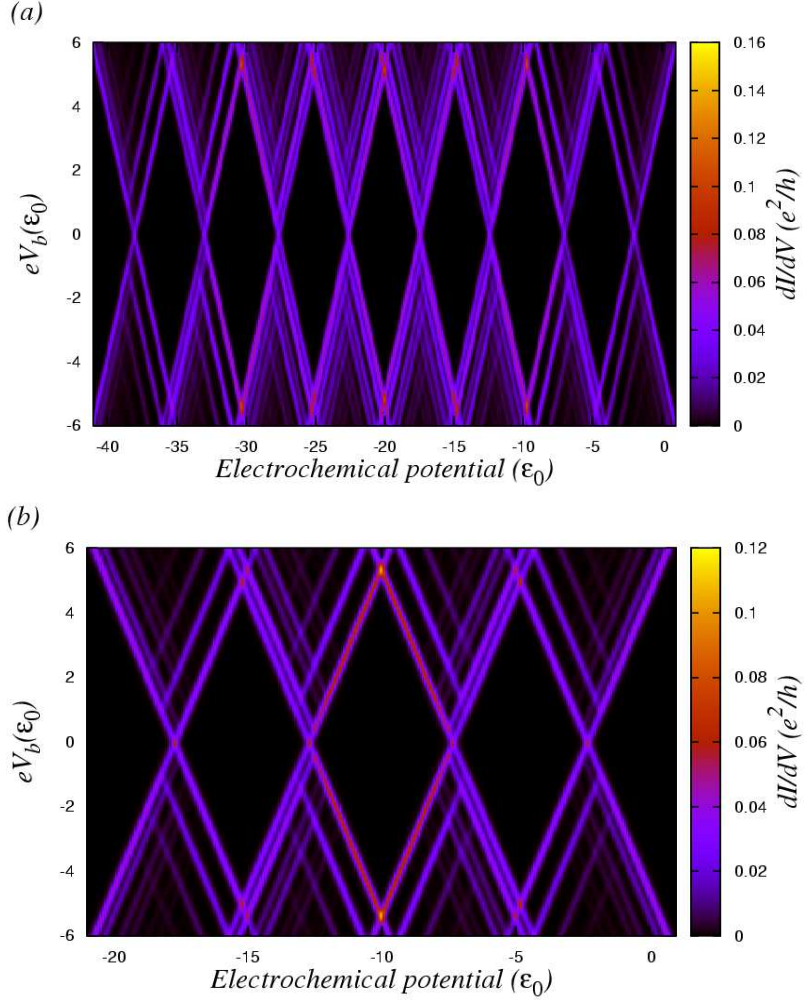


FIG. 7: (Color online) Calculated stability diagrams of double-walled carbon nanotube (DWCNT) quantum dot (QD) systems. (a) Stability diagram of a commensurate DWCNT(c-DWCNT) QD. The parameters are $\Delta = 0.2$, $\zeta = 0.3$, $W_{00}^{++} = W_{00}^{--} = W_{00}^{+-}/2 = 5.0\varepsilon_0$ and $k_B T = 0.05\varepsilon_0$, where the level spacing ε_0 is used as the unit of energy. We use $\gamma_{s\pm} = \gamma_{d\pm} = 0.01\varepsilon_0$ for the coupling strengths between the leads and the DWCNT QD. (b) Stability diagram of an incommensurate DWCNT(i-DWCNT) QD. The parameters are $\Delta_+ = 0.2$, $\Delta_- = 0.3$, $W_{00}^{++} = 5\varepsilon_0$, $W_{00}^{--} = 6.0\varepsilon_0$, $W_{00}^{+-} = 5.5\varepsilon_0$ and $k_B T = 0.05\varepsilon_0$. The coupling strengths are $\gamma_{s+} = \gamma_{d+} = 0.01\varepsilon_0$ and $\gamma_{s-} = \gamma_{d-} = 0$. The size of the Coulomb diamonds shows an 8-electron periodicity in c-DWCNT QDs as shown in (a) while it shows a 4-electron periodicity in i-DWCNT QDs as shown in (b).

diamonds shows an 8-electron periodicity in c-DWCNT QDs and an 4-electron periodicity in i-DWCNT QDs. The excitation lines are also shown in Fig. 7, which contain contributions of both fermionic (cf. Eqs. (31) and (32)) and bosonic excitations (cf. Eq. (42)). There are more excitation lines in c-DWCNT QDs than in i-DWCNT QDs because of the larger number of the ground states of c-DWCNTs. The stability diagram of an i-DWCNT QD looks quite similar to that of a SWCNT QD, which shows also a 4-electron periodicity. However, the configuration of the excitation lines of the two cases are different, because the excitation spectrum in i-DWCNTs contains an extra contribution from the Coulomb interaction due to the electrons in the inner shell.

V. CONCLUSIONS

In this paper, we derive the energy spectrum of both finite length c-DWCNTs and i-DWCNTs with open boundary conditions. Then we calculate the transport properties of the DWCNT QD system by solving the Bloch-Redfield equations for the reduced density matrix of the QD systems. Because the contacts are usually deposited on the outer shell and the intershell coupling depends on the chiralities of the two shells, we find an 8-electron periodicity of the linear conductance peak distances in c-DWCNTs but a 4-electron periodicity in i-DWCNTs. The peak heights

strongly depend on the degeneracies of the ground states. By including both fermionic and bosonic excitations, we also calculate the stability diagrams of QD systems with both c-DWCNTs and i-DWCNTs in an inelastic tunneling process. The periodicity of the Coulomb diamond sizes depends on the number of the shells contributing to the electron transport. Therefore, the 4-electron periodicity in a MWCNT QD measured in the experiments in Ref. 21 may be due to the fact that only the outermost metallic shell was involved in the electron transport. Similarly, the 4-electron periodicity in i-DWCNTs is because of the negligible intershell coupling and there will be an 8-electron periodicity if a large intershell coupling is caused for example by contacts. Therefore, it's necessary to use properly prepared contacts in order to observe the different periodicities of Coulomb blockade oscillations in different types of DWCNTs in the experiments.

Acknowledgments

The authors would like to thank L. Mayrhofer for helpful discussions. The authors acknowledge the support of DFG under the program GRK 638.

APPENDIX A: MATRIX ELEMENTS OF THE ELECTRON OPERATORS

In this appendix, we calculate the matrix elements of the electron operators Eqs. (22) and (27) in the basis of the eigenstates, Eq. (43), of the Hamiltonian H_{QD} and the results are used in Sec. III. The matrix elements of the electron operator are calculated by using the relations

$$\langle \mathbf{N}, \mathbf{m} | \Psi_{\alpha\sigma}(\mathbf{r}) | \mathbf{N}', \mathbf{m}' \rangle = \sqrt{L} \sum_{\tilde{r}F} \text{sgn}(F) \varphi_{\alpha \text{sgn}(F) \tilde{r}F}(\mathbf{r}) \langle \mathbf{N}, \mathbf{m} | \psi_{\alpha\tilde{r}\sigma F}(u) | \mathbf{N}', \mathbf{m}' \rangle. \quad (\text{A1})$$

The 1D electron operator $\psi_{\alpha\tilde{r}\sigma}$ can be expressed in terms of the bosonic operators introduced above as^{31,32}

$$\psi_{\alpha\tilde{r}\sigma}(u) = \frac{\eta_{\alpha\tilde{r}\sigma} K_{\alpha\tilde{r}\sigma}(u)}{\sqrt{1 - e^{-a\pi/L}}} e^{i\phi_{\alpha\tilde{r}\sigma}^\dagger(u) + i\phi_{\alpha\tilde{r}\sigma}(u)}, \quad (\text{A2})$$

where a is an infinitesimal positive number used to avoid the divergence in the long wave length limit and the operator $\eta_{\alpha\tilde{r}\sigma}$ is the Klein factor, which destroys a particle in the branch $\alpha\tilde{r}\sigma$ when acting on the eigenstates of the DWCNT Hamiltonian,

$$\eta_{\alpha\tilde{r}\sigma} | \mathbf{N}, \mathbf{m} \rangle = (-1)^{\sum_{i=1}^{\alpha\tilde{r}\sigma-1} N_i} | \mathbf{N} - \mathbf{e}_{\alpha\tilde{r}\sigma}, \mathbf{m} \rangle,$$

where we use the convention $i = +\tilde{R}\uparrow, +\tilde{L}\uparrow, +\tilde{R}\downarrow, +\tilde{L}\downarrow, -\tilde{R}\uparrow, -\tilde{L}\uparrow, -\tilde{R}\downarrow, -\tilde{L}\downarrow = 1, 2, 3, 4, 5, 6, 7, 8$ and the vector $\mathbf{e}_{\alpha\tilde{r}\sigma}$ denotes a state where there is only one particle in the branch $\alpha\tilde{r}\sigma$. The notation $\sum_{i=1}^{\alpha\tilde{r}\sigma-1}$ means that the sum runs over all the state from 1 to $i = \alpha\tilde{r}\sigma - 1$ with $\alpha\tilde{r}\sigma$ fixed by the unit vector $\mathbf{e}_{\alpha\tilde{r}\sigma}$. The phase factor is

$$K_{\alpha\tilde{r}\sigma}(u) = \frac{1}{\sqrt{2L}} e^{i\frac{\pi}{L} \text{sgn}(F) (\text{sgn}(\tilde{r}) N_{\alpha\tilde{r}\sigma} + \Delta_\alpha) u},$$

where $\Delta_\pm = \Delta$ for the c-DWCNTs. The field operator $\phi_{\alpha\tilde{r}\sigma}^\dagger$ is given as

$$i\phi_{\alpha\tilde{r}\sigma}(u) = \sum_{q>0} \frac{e^{-aq/2}}{\sqrt{n_q}} e^{i \text{sgn}(\tilde{r}F) qu} b_{\alpha \text{sgn}(\tilde{r}) q \sigma}.$$

Therefore, the matrix elements of the 1D electron operator have the form¹⁹

$$\langle \mathbf{N}, \mathbf{m} | \psi_{\alpha\tilde{r}\sigma}(u) | \mathbf{N}', \mathbf{m}' \rangle = \delta_{\mathbf{N} + \mathbf{e}_{\alpha\tilde{r}\sigma}, \mathbf{N}'} \frac{(-1)^{\sum_{i=1}^{\alpha\tilde{r}\sigma-1} N_i}}{\sqrt{1 - e^{-a\pi/L}}} K_{\alpha\tilde{r}\sigma}(u) \prod_{q>0} \prod_{j\delta\xi} F(\lambda_{\alpha\tilde{r}\sigma q}^{j\delta\xi F}(u), m_{j\delta\xi q}, m'_{j\delta\xi q}), \quad (\text{A3})$$

where the function F can be expressed in terms of the Laguerre polynomials L_m^n ⁴⁰

$$F(\lambda, m, m') = \frac{m_{\min}!}{m_{\max}!} L_{m_{\min}}^{m_{\max} - m_{\min}}(|\lambda|^2) \left(\Theta(m' - m) \lambda^{m' - m} + \Theta(m - m') (-\lambda^*)^{m - m'} \right) \quad (\text{A4})$$

with $m_{\max} = \max(m, m')$ and $m_{\min} = \min(m, m')$. $\Theta(x)$ is the Heaviside step function and the parameters λ 's are given by

$$\lambda_{\alpha\tilde{r}\sigma q}^{j\delta\xi F}(u) = \frac{\Lambda_{\alpha\tilde{r}\sigma}^{j\delta\xi q}}{\sqrt{n_q}} \left(e^{i \text{sgn}(\tilde{r}F) qu} S_{j\delta\xi q} - e^{-i \text{sgn}(\tilde{r}F) qu} C_{j\delta\xi q} \right). \quad (\text{A5})$$

APPENDIX B: EXPRESSIONS OF THE TUNNELING RATES

In this appendix, we give a derivation of the expressions of the tunneling rates, Eqs. (53) and (54). In general, the expressions of the tunneling rates Γ 's are given by¹⁹,

$$\Gamma_{lk'mnk}^{(\pm)E_N E_{N+1}} = \frac{1}{\hbar^2} \sum_{\alpha\sigma} \iint d\mathbf{x}d\mathbf{y} \left(\Psi_{\alpha\sigma}(\mathbf{x}) \right)_{k'm}^{E_N E'_{N+1}} \left(\Psi_{\alpha\sigma}^\dagger(\mathbf{y}) \right)_{nk}^{E'_{N+1} E_N} \times \int_0^\infty dt' \mathcal{F}_{l\alpha\sigma}(\mathbf{x}, \mathbf{y}, t') e^{\mp \frac{i}{\hbar}(E'_{N+1} - E_N)t'}, \quad (\text{B1})$$

$$\Gamma_{lk'mnk}^{(\pm)E_N E_{N-1}} = \frac{1}{\hbar^2} \sum_{\alpha\sigma} \iint d\mathbf{x}d\mathbf{y} \left(\Psi_{\alpha\sigma}^\dagger(\mathbf{x}) \right)_{k'm}^{E_N E'_{N-1}} \left(\Psi_{\alpha\sigma}(\mathbf{y}) \right)_{nk}^{E'_{N-1} E_N} \times \int_0^\infty dt' \mathcal{E}_{l\alpha\sigma}(\mathbf{x}, \mathbf{y}, t') e^{\mp \frac{i}{\hbar}(E'_{N-1} - E_N)t'}, \quad (\text{B2})$$

where $t' = t - t_1$. The two functions are defined as

$$\begin{aligned} \mathcal{E}_{l\alpha\sigma}(\mathbf{x}, \mathbf{y}, t') &= T_{l\alpha}(\mathbf{x})T_{l\alpha}^*(\mathbf{y}) \left\langle \Phi_{l\sigma}(\mathbf{x})\Phi_{l\sigma}^\dagger(\mathbf{y}, -t') \right\rangle_{\text{th}} \\ &= T_{l\alpha}(\mathbf{x})T_{l\alpha}^*(\mathbf{y}) \int d\varepsilon g_l(\varepsilon)(1 - f(\varepsilon)) \sum_{\mathbf{q}} \phi_{\mathbf{q}}(\mathbf{x})\phi_{\mathbf{q}}^*(\mathbf{y}) e^{-\frac{i}{\hbar}(\varepsilon - eV_l)t'}, \end{aligned} \quad (\text{B3})$$

$$\begin{aligned} \mathcal{F}_{l\alpha\sigma}(\mathbf{x}, \mathbf{y}, t') &= T_{l\alpha}^*(\mathbf{x})T_{l\alpha}(\mathbf{y}) \left\langle \Phi_{l\sigma}^\dagger(\mathbf{x})\Phi_{l\sigma}(\mathbf{y}, -t') \right\rangle_{\text{th}} \\ &= T_{l\alpha}^*(\mathbf{x})T_{l\alpha}(\mathbf{y}) \int d\varepsilon g_l(\varepsilon)f(\varepsilon) \sum_{\mathbf{q}} \phi_{\mathbf{q}}^*(\mathbf{x})\phi_{\mathbf{q}}(\mathbf{y}) e^{\frac{i}{\hbar}(\varepsilon - eV_l)t'}, \end{aligned} \quad (\text{B4})$$

where $g_l(\varepsilon)$ is the density of states in lead l , V_l is the voltage in the lead l , and $f(\varepsilon)$ is the Fermi distribution function. In the following we shall derive the expressions for the tunneling rates $\Gamma_{lk'mnk}^{(\pm)E_N E_{N+1}}$ for an i-DWCNT QD system as an example and the expressions for the other tunneling rates can be obtained by the same method. By substituting Eqs. (B4) and (22) into Eq. (B1), we have

$$\begin{aligned} \Gamma_{lk'mnk}^{(\pm)E_N E_{N+1}} &= \frac{\pi L}{\hbar} \sum_{\alpha\sigma} \sum_{\tilde{r}\tilde{r}'} \sum_{FF'} \text{sgn}(FF') \iint d\mathbf{x}d\mathbf{y} \varphi_{\alpha\text{sgn}(F)\tilde{r}F}(\mathbf{x})\varphi_{\alpha\text{sgn}(F')\tilde{r}'F'}^*(\mathbf{y}) \\ &\quad \times g_l(\varepsilon_l)f(\varepsilon_l)T_{l\alpha}^*(\mathbf{x})T_{l\alpha}(\mathbf{y}) \sum_{\mathbf{q}} \phi_{\mathbf{q}}^*(\mathbf{x})\phi_{\mathbf{q}}(\mathbf{y}) \\ &\quad \times \left(\psi_{\alpha\tilde{r}\sigma F}(u_l) \right)_{k'm}^{E_N E'_{N+1}} \left(\psi_{\alpha\tilde{r}'\sigma F'}(u_l) \right)_{nk}^{E'_{N+1} E_N}, \end{aligned} \quad (\text{B5})$$

where $\varepsilon_l = eV_l - E_N - E_{N+1}$ and $u_l = 0, L$ for $l = s, d$. We ignore the slow oscillations of the 1D electron operators along the length of the tunneling interfaces and therefore the product $\left(\psi_{\alpha\tilde{r}\sigma F}(u_l) \right)_{k'm}^{E_N E'_{N+1}} \left(\psi_{\alpha\tilde{r}'\sigma F'}(u_l) \right)_{nk}^{E'_{N+1} E_N}$ is independent of the positions. The integrals over ε and t' are carried out by using

$$\int d\varepsilon g_l(\varepsilon) \int_0^\infty dt' e^{\pm \frac{i}{\hbar}(\varepsilon - E)t'} = \pi \hbar g(E) \pm i \hbar \mathcal{P} \int \frac{g(\varepsilon)}{\varepsilon - E} d\varepsilon$$

with \mathcal{P} denotes the Cauchy principal value. We assume that the width of the lead energy band is infinite and that the lead density of states $g_l(\varepsilon)$ is constant. Hence the Cauchy principal value is zero. Let's focus on the part depending on the position in Eq. (B5), namely,

$$I = \iint d\mathbf{x}d\mathbf{y} \varphi_{\alpha\text{sgn}(F)\tilde{r}F}(\mathbf{x})\varphi_{\alpha\text{sgn}(F')\tilde{r}'F'}^*(\mathbf{y})T_{l\alpha}^*(\mathbf{x})T_{l\alpha}(\mathbf{y}) \sum_{\mathbf{q}} \phi_{\mathbf{q}}^*(\mathbf{x})\phi_{\mathbf{q}}(\mathbf{y}). \quad (\text{B6})$$

Because the Bloch waves $\varphi_{\alpha\text{sgn}(F)\tilde{r}F}$ from Eq. (6) are largely localized around the carbon atoms and on the length scale of the p_z orbitals all the other quantities in Eq. (B6) are slowly varying, we can rewrite the two integrals as two sums over the positions of the carbon atoms and the Eq. (B6) becomes

$$I = \frac{C}{N_\alpha} \sum_{\mathbf{R}\mathbf{p}} \sum_{\mathbf{R}'\mathbf{p}'} e^{i\mathbf{F}\cdot\mathbf{R}} e^{i\mathbf{F}'\cdot\mathbf{R}'} f_{\alpha\text{psgn}(F)\tilde{r}F} f_{\alpha\text{psgn}(F')\tilde{r}'F'}^* T_{l\alpha}^*(\mathbf{x}_{\mathbf{R},\mathbf{p}}) T_{l\alpha}(\mathbf{y}_{\mathbf{R}',\mathbf{p}'}) \sum_{\mathbf{q}} \phi_{\mathbf{q}}^*(\mathbf{x}_{\mathbf{R},\mathbf{p}}) \phi_{\mathbf{q}}(\mathbf{y}_{\mathbf{R}',\mathbf{p}'}), \quad (\text{B7})$$

where the constant C denotes the integration over the p_z orbitals. Because the leads are described by 3D Fermi gases, the wave functions $\phi_{l\mathbf{q}}(\mathbf{x})$ are the plane waves,

$$\phi_{l\mathbf{q}}(\mathbf{x}) = \frac{1}{\sqrt{V_l}} e^{i\mathbf{q}\cdot\mathbf{x}}$$

with the volume of the gas V_l . The sum over \mathbf{q} can be performed

$$\sum_{\mathbf{q}} \phi_{\mathbf{q}}^*(\mathbf{x}) \phi_{\mathbf{q}}(\mathbf{y}) \approx \frac{4\pi \sin(|\mathbf{q}||\mathbf{x} - \mathbf{y}|)}{|\mathbf{q}||\mathbf{x} - \mathbf{y}|},$$

which is peaked around $\mathbf{x} = \mathbf{y}$. Because of the large Fermi energy in the leads, the above expression can be approximated by two Kronecker δ 's,

$$\sum_{\mathbf{q}} \phi_{\mathbf{q}}^*(\mathbf{x}_{\mathbf{R},p}) \phi_{\mathbf{q}}(\mathbf{y}_{\mathbf{R}',p'}) \approx 4\pi \delta_{\mathbf{R}\mathbf{R}'} \delta_{pp'}.$$

Therefore, Eq. (B7) becomes

$$I = \frac{C}{N_\alpha} \sum_{\mathbf{R}p} e^{(i\mathbf{F}-\mathbf{F}')\cdot\mathbf{R}} f_{\alpha p \text{sgn}(F)\tilde{r}F} f_{\alpha p \text{sgn}(F')\tilde{r}'F'}^* T_{l\alpha}^*(\mathbf{x}_{\mathbf{R},p}) T_{l\alpha}(\mathbf{y}_{\mathbf{R},p}). \quad (\text{B8})$$

Because of the fast oscillating phase $e^{(i\mathbf{F}-\mathbf{F}')\cdot\mathbf{R}}$, the quantity I is nonzero only if $F = F'$ and in turn the sum over p can be carried out as

$$\sum_p f_{\alpha p \text{sgn}(F)\tilde{r}F} f_{\alpha p \text{sgn}(F)\tilde{r}'F}^* = \delta_{\tilde{r}\tilde{r}'},$$

which can be easily verified by using the explicit expressions Eqs (7) and (8). Eq. (B8) becomes

$$I = \frac{C}{N_\alpha} \sum_{\mathbf{R}p} T_{l\alpha}^*(\mathbf{x}_{\mathbf{R},p}) T_{l\alpha}(\mathbf{y}_{\mathbf{R},p}) \delta_{FF'} \delta_{\tilde{r}\tilde{r}'}. \quad (\text{B9})$$

By substituting Eq. (B9) and Eq. (A3) of the matrix elements of the electron operators into Eq. (B5), we finally obtain the expression of the tunneling rates,

$$\begin{aligned} \Gamma_{lk'mnk}^{(\pm)E_N E_{N+1}} &= \sum_{\alpha} \frac{\gamma_{l\alpha}}{h} g_l(\varepsilon_l) f(\varepsilon_l) \sum_{\tilde{r}\sigma F} \delta_{\mathbf{N}+\mathbf{e}_{\alpha\tilde{r}\sigma}, \mathbf{N}+1} \prod_{q>0} \prod_{q'>0} \prod_{j\delta\xi} \prod_{j'\delta'\xi'} \\ &\times F(\lambda_{\alpha\tilde{r}\sigma q}^{j\delta\xi F}(u_l), k'_{j\delta\xi q}, m_{j\delta\xi q}) F^*(\lambda_{\alpha\tilde{r}\sigma q}^{j'\delta'\xi' F}(u_l), n_{j'\delta'\xi' q'}, k_{j'\delta'\xi' q'}), \end{aligned} \quad (\text{B10})$$

where the vector $\mathbf{e}_{\alpha\tilde{r}\sigma}$ denotes a state with one particle in the branch $\alpha\tilde{r}\sigma$. The function $F(\lambda, m, m')$ is given in Eq. (A4) and the parameters $\lambda_{\alpha\tilde{r}\sigma}^{j\delta\xi F}$'s are defined in Eq. (A5). The constants $\gamma_{l\alpha}$ describes the coupling strengths between the shell α in i-DWCNTs and the leads l having the form

$$\gamma_{l\alpha} = \pi^2 C \sum_{\mathbf{R}p} \frac{|T_{l\alpha}(\mathbf{x}_{\mathbf{R},p})|^2}{1 - e^{-a\pi/L}},$$

The four eigenstates are

$$\begin{aligned} |k'\rangle &= |\mathbf{N}, \mathbf{k}'\rangle, & |m\rangle &= |\mathbf{N} + \mathbf{1}, \mathbf{m}\rangle, \\ |n\rangle &= |\mathbf{N} + \mathbf{1}, \mathbf{n}\rangle, & |k\rangle &= |\mathbf{N}, \mathbf{k}\rangle. \end{aligned}$$

Similarly, the expressions for the other tunneling rates are

$$\begin{aligned} \Gamma_{lk'mnk}^{(\pm)E_N E_{N-1}} &= \sum_{\alpha} \frac{\gamma_{l\alpha}}{h} g_l(\varepsilon_l) (1 - f(\varepsilon_l)) \sum_{\tilde{r}\sigma F} \delta_{\mathbf{N}-\mathbf{e}_{\alpha\tilde{r}\sigma}, \mathbf{N}-1} \prod_{q>0} \prod_{q'>0} \prod_{j\delta\xi} \prod_{j'\delta'\xi'} \\ &\times F^*(\lambda_{\alpha\tilde{r}\sigma q}^{j\delta\xi F}(u_l), k'_{j\delta\xi q}, m_{j\delta\xi q}) F(\lambda_{\alpha\tilde{r}\sigma q}^{j'\delta'\xi' F}(u_l), n_{j'\delta'\xi' q'}, k_{j'\delta'\xi' q'}) \end{aligned} \quad (\text{B11})$$

with the eigenstates

$$\begin{aligned} |k'\rangle &= |\mathbf{N}, \mathbf{k}'\rangle, & |m\rangle &= |\mathbf{N} - \mathbf{1}, \mathbf{m}\rangle, \\ |n\rangle &= |\mathbf{N} - \mathbf{1}, \mathbf{n}\rangle, & |k\rangle &= |\mathbf{N}, \mathbf{k}\rangle. \end{aligned}$$

From the expressions of the tunneling rate, Eqs. (B10) and (B11), we can see clearly that the contacts do not mix the electrons in different branches.

-
- ¹ S. Ijima, *Nature* **354**, 56 (1991).
² R. Saito, G. Dresselhaus, and M. S. Dresselhaus, *Physical Properties of Carbon Nanotubes* (Imperial College Press, London, 1998).
³ J.-C. Charlier, X. Blase, and S. Roche, *Rev. Mod. Phys.* **79**, 677 (2007).
⁴ A. Loiseau, P. Launois, P. Petit, S. Roche, and J. Salvetat, eds., *Understanding Carbon Nanotubes*, vol. 677 of *Lecture Notes in Physics* (Springer Berlin, 2006).
⁵ R. Egger and A. O. Gogolin, *Phys. Rev. Lett.* **79**, 5082 (1997).
⁶ R. Egger and A. O. Gogolin, *Eur. Phys. J. B* **3**, 281 (1998).
⁷ C. Kane, L. Balents, and M. P. A. Fisher, *Phys. Rev. Lett.* **79**, 5086 (1997).
⁸ M. Bockrath, D. H. Cobden, J. Lu, A. G. Rinzler, R. E. Smalley, L. Balents, and P. L. McEuen, *Nature* **397**, 598 (1999).
⁹ H. Postma, T. Teepen, Z. Yao, M. Grifoni, and C. Dekker, *Science* **293**, 76 (2001).
¹⁰ W. Liang, M. Bockrath, and H. Park, *Phys. Rev. Lett.* **88**, 126801 (2002).
¹¹ S. Moriyama, T. Fuse, M. Suzuki, Y. Aoyagi, and K. Ishibashi, *Phys. Rev. Lett.* **94**, 186806 (2005).
¹² S. Sapmaz, P. Jarillo-Herrero, J. Kong, C. Dekker, L. P. Kouwenhoven, and H. S. J. van der Zant, *Phys. Rev. B* **71**, 153402 (2005).
¹³ S. Sapmaz, P. Jarillo-Herrero, L. Kouwenhoven, and H. van der Zant, *Semicond. Sci. Technol* **21**, S52 (2006).
¹⁴ H. Grabert and M. Devoret, eds., *Single Electron Tunneling* (Plenum, New York, 1991).
¹⁵ Y. Alhassid, *Rev. Mod. Phys.* **72**, 895 (2000).
¹⁶ D. H. Cobden and J. Nygård, *Phys. Rev. Lett.* **89**, 046803 (2002).
¹⁷ Y. Oreg, K. Byczuk, and B. I. Halperin, *Phys. Rev. Lett.* **85**, 365 (2000).
¹⁸ L. Mayrhofer and M. Grifoni, *Phys. Rev. B* **74**, 121403(R) (2006).
¹⁹ L. Mayrhofer and M. Grifoni, *Eur. Phys. J. B* **57**, 107 (2007).
²⁰ L. Mayrhofer and M. Grifoni, in preparation.
²¹ M. R. Buitelaar, A. Bachtold, T. Nussbaumer, M. Iqbal, and C. Schönenberger, *Phys. Rev. Lett.* **88**, 156801 (2002).
²² Y.-G. Yoon, P. Delaney, and S. G. Louie, *Phys. Rev. B* **66**, 073407 (2002).
²³ S. Roche, F. Triozon, A. Rubio, and D. Mayou, *Phys. Rev. B* **64**, 121401(R) (2001).
²⁴ F. Triozon, S. Roche, A. Rubio, and D. Mayou, *Phys. Rev. B* **69**, 121410(R) (2004).
²⁵ S. Wang and M. Grifoni, *Phys. Rev. Lett.* **95**, 266802 (2005).
²⁶ R. Egger, *Phys. Rev. Lett.* **83**, 5547 (1999).
²⁷ R. Saito, G. Dresselhaus, and M. S. Dresselhaus, *J. Appl. Phys.* **73**, 494 (1993).
²⁸ S. Uryu, *Phys. Rev. B* **69**, 075402 (2004).
²⁹ S. Uryu and T. Ando, *Phys. Rev. B* **72**, 245403 (2005).
³⁰ F. Haldane, *J. Phys. C* **14** (1981).
³¹ J. Voit, *Rep. Prog. Phys.* **57**, 977 (1994).
³² J. von Delft and H. Schoeller, *Annalen der Physik* **4**, 225 (1998).
³³ T. Giamarchi, *Quantum physics in one dimension* (Oxford university press, 2004).
³⁴ K. A. Matveev and L. I. Glazman, *Phys. Rev. Lett.* **70**, 990 (1993).
³⁵ K. Blum, *Density Matrix Theory and Applications* (Plenum Press, New York, 1996).
³⁶ F. Bloch, *Phys. Rev.* **105**, 1206 (1957).
³⁷ A. Redfield, *IBM J. Res. Dev* **1**, 19 (1957).
³⁸ L. I. Glazman and K. A. Matveev, *JETP Lett* **48**, 445 (1988).
³⁹ C. W. J. Beenakker, *Phys. Rev. B* **44**, 1646 (1991).
⁴⁰ I. S. Gradshteyn and I. Ryzhik, *Table of Integral, Series and Products* (Academic Press, San Diego, 2000).